

New mechanisms for forming multiple hotspots in radio jets

Maya A. Horton ¹, ²★, Martin G. H. Krause ² and Martin J. Hardcastle ²

Centre for Astrophysics Research, Department of Physics, Astronomy and Mathematics, University of Hertfordshire, College Lane, Hatfield AL10 9AB, UK

Accepted 2023 February 27. Received 2023 February 27; in original form 2022 May 9

ABSTRACT

Hotspots of radio galaxies are regions of shock-driven particle acceleration. Multiple hotspots have long been identified as potential indicators of jet movement or precession. Two frequent explanations describe a secondary hotspot as either the location of a prior jet termination point or a deflected backflow-driven shock: the so-called dentist’s drill and splatter-spot models. We created high-resolution simulations of precessing jets with a range of parameters. In addition to the existing mechanisms, our results show three additional mechanisms for multiple hotspot formation: (1) the splitting of a large terminal hotspot into passive and active components; (2) jet stream splitting resulting in two active hotspots; and (3) dynamic multiple hotspot complexes that form as a result of jet termination in a turbulent cocoon, linked here to rapid precession. We show that these distinct types of multiple hotspots are difficult to differentiate in synthetic radio maps, particularly hotspot complexes that can easily be mistaken for the jet itself. We discuss the implication for hypothesized binary supermassive black hole systems where jet precession is a key component of the morphology, and show a selection of potential precession candidates found using the Low-Frequency Array Two-metre Sky Survey Data Release 2.

Key words: black hole physics – hydrodynamics – methods: numerical – galaxies: active – galaxies: jets.

1 INTRODUCTION

Hotspots are considered to be a defining characteristic of Fanaroff and Riley (Fanaroff & Riley 1974) class II (FR II) radio sources (Carilli, Bartel & Linfield 1995). However, from the earliest observations it has been clear that their shape and complexity do not easily fit with simple descriptions of them as planar shocks: while there is little doubt that they are regions of shock-driven particle acceleration occurring at the termination points of edge-brightened radio sources (e.g. Laing 1989), their shape and complexity can be difficult to categorize.

Many FR II sources have multiple hotspots (e.g. Laing 1982; Leahy et al. 1997), although it is generally expected that a jet can only have one current termination point. Two primary mechanisms for forming multiple hotspots are described in the literature. In the ‘dentist’s drill’ model (Scheuer 1982; Hardee & Norman 1990; Cox, Gull & Scheuer 1991), the jet changes direction, either through precession or through a discontinuous reorientation (Ekers et al. 1978), on a time-scale shorter than that required for the initial hotspot to fade. Under the ‘splatter-spot’ model, a secondary shock is generated by continued supersonic collimated outflow from the initial jet termination point, perhaps after the jet is deflected obliquely by the lobe boundary (the contact discontinuity between jet plasma and shocked ambient medium; Smith 1984; Williams 1985; Lonsdale & Barthel 1986).

Observationally, both of these models have difficulty explaining the diversity of hotspot structures observed in real radio galaxies. Both predict that the jet should currently terminate in a compact ‘primary’ hotspot and that other (‘secondary’) hotspots should be more diffuse. In the simplest version of the dentist’s drill model, the

secondary hotspot should show signs of spectral ageing relative to the primary, but this is not observed in some well-studied cases (Hardcastle & Looney 2001); the properties of many secondary hotspots are not consistent with being older, remnant versions of the primaries (Valtaoja 1984). Models involving a decelerated continued outflow predict that the secondary hotspot should always be downstream of the primary, and should have less efficient particle acceleration, but this is not consistent with observations showing that particle acceleration can be as efficient in the secondary as in the primary (Hardcastle, Croston & Kraft 2007).

The formation mechanisms of multiple hotspots are particularly important because of their role as indicators for jet precession or reorientation (Krause et al. 2019). Jet precession, if caused by the geodetic precession of binary supermassive black holes (e.g. Begelman, Blandford & Rees 1980; Gower et al. 1982), can be used as an indicator of the prevalence of such systems, which are progenitors of high-energy gravitational wave events. Additionally, jet precession can be caused by other mechanisms such as Lense–Thirring or Bardeen–Petterson (e.g. Lense & Thirring 1918; Bardeen & Petterson 1975) and these are also expected to have observational signatures. Previous simulation-based work has often used more or less realistic precession models to generate multiple hotspots (e.g. Cox et al. 1991).

In a previous paper, Horton, Krause & Hardcastle (2020b) used high-resolution hydrodynamic simulations to investigate the effects of precession on the observable properties of jets in radio galaxies, showing that curved, S-shaped and misaligned jets are reliable precession indicators. A systematic study of hotspots was excluded from that paper, given their complexity. Here, we report on highest resolution simulations of such systems that allow us to study the formation of multiple hotspots directly. We identify three

* E-mail: mh17adw@herts.ac.uk

novel, precession-driven hydrodynamic processes that may result in the formation of multiple hotspots whose properties would not be inconsistent with observations of spectral ageing and particle acceleration and help to explain discrepancies in size and position between ‘primary’ and ‘secondary’ hotspots. These are in addition to the existing two mechanisms. Finally, we briefly discuss physical mechanisms that can lead to jet precession, and discuss how some of these can have an impact on the search for supermassive binary black hole systems; as Horton et al. (2020a) highlight, terminal hotspots are particularly important in the use of statistical models to constrain binary separations and gravitational wave strains using precessing jets (see also Krause et al. 2019).

2 METHODS

2.1 Simulations

We use the simulation set-up described by Horton et al. (2020b) – hereafter referred to as H20 – using the PLUTO hydrodynamic code¹ (Mignone et al. 2007) running the hydrodynamics (HD) physics module with a Hartan-Lax-van Leer contact (HLLC) Riemann solver and second-order Runge–Kutta time-stepping with PLUTO’s ‘linear’ reconstruction that is second-order accurate in space. Higher order spatial reconstruction or time-stepping significantly increases the computational cost for high-resolution simulations. We chose to work in HD rather than magnetohydrodynamics (MHD) or relativistic hydrodynamics (RHD) partly for computational simplicity and the efficient use of a spherical grid: previous work (e.g. Hardcastle & Krause 2014) has demonstrated that the use of realistic subequipartition fields has no global effect on the lobe or jet dynamics, and although we expect bulk flow speeds to be relativistic in real jets, the flows downstream of shocks that are the topic of this paper will be at most mildly relativistic.

The supersonic ($M = 100$) jet was injected as a spot moving on the intersection between a specified precession cone and the inner boundary of the spherical computational volume. The extent of the linear grid in code units was $0.2 \leq r \leq 5$, $0 \leq \theta \leq \pi$, and $0 \leq \phi \leq 2\pi$. This paper uses two of the .VHR (very high resolution) simulation runs described in H20 with a grid set-up of $512 \times 512 \times 1024$ in spherical polar coordinates of r (radial), θ (polar), and ϕ (azimuthal) angles, respectively. This angular resolution means that the 5° injection spots are well resolved with ~ 300 grid elements across each spot.

The initial jet density and pressure are set to match those of the ambient environment, but the conical jet injection described by H20 has the feature that the jet naturally expands and then recollimates and heats up within a short distance from the injection location, as expected in theoretical models (Kaiser & Alexander 1997), while remaining supersonic ($M \sim 10$). The jets and lobes on large scales are therefore hot and low density with respect to their environment, matching at least qualitatively what is expected for real radio galaxies (Hardcastle & Krause 2013). As discussed by H20, the simulations are intrinsically scale free but if we assume a plausible environment for radio galaxies and set the outer radius of the simulations to 300 kpc, then the simulation unit of distance is 60 kpc, the sound speed is 480 km s^{-1} , and one simulation time unit is $1.2 \times 10^8 \text{ yr}$, while the time-step between saved simulation volumes is $1.2 \times 10^5 \text{ yr}$. The jet power is then well matched to the expected powers of FR II radio galaxies.

The parameters varied were precession period pp and precession cone opening angle ψ . All jets had a fixed half-cone angle (ϕ) of 5° ; pp was set at either 1 or 5 turns per simulation time (i.e. pps in physical units, using the above conversions, in the range of 10^7 – 10^8 yr) and ψ was set at 45° . These runs were selected from H20 because the wide precession cone opening angle gave rise to interesting behaviour regardless of how many turns there were over the lifetime of the source. Because of this choice, we are modelling relatively slow precession but, as discussed by H20, we expect that the qualitative behaviour we observe in simulated radio morphology will not be strongly dependent on the pp . We did not vary the injection Mach number M nor examine intermediate values of ψ as set out in H20 as this would have required additional VHR runs. As in the previous paper, jets were injected into a uniform environment. We did not run jets for more than one simulation time. No other parameters were altered for .VHR runs (in the bulk of this paper, we analyse only 45_100_1_VHR and 45_100_02_VHR, out of the four original simulations). We also ran a VHR straight jet, 15_100_STR_VHR, to see whether the same hydrodynamic effects appeared without precession. Movies showing the evolution of the pressure contours for these simulations can be found at https://uhhpc.herts.ac.uk/~may_aahorton/multihotspots.html.

We recognize that the term ‘hotspot’ is often closely associated with flat spectral indices; the spectral index of the radio galaxies is not modelled here. However, modelled emissivity is a strong proxy for pressure excesses associated with shocks and sites of particle acceleration associated with true radio hotspots. More studies taking into account particle acceleration are required to confirm whether these structures would genuinely form visible hotspots.

The jets were visualized using YT² for PYTHON. To do this, we converted the PLUTO computational volume, in spherical polars, to a uniform three-dimensional 1025^3 Cartesian grid using simple nearest pixel interpolation. The Cartesian grid is matched in resolution to the radial resolution of the spherical computational domain but does not resolve the details of the jet structures close to the injection region. It is, however, more than adequate to sample the spherical volume elements at large distances from the injection region. The Cartesian grids were read into YT using the `load_uniform_grid` function.

A proxy for synchrotron emission in the lobes was obtained by taking pressure to a fixed power (1.8) as described in H20 and masking with a tracer threshold of 10^{-3} . We used the following three distinct YT functions:

(i) `yt.create_scene`: This is used to create three-dimensional contour maps of pressure in the lobes and the surrounding medium as seen from a point outside the computational volume. We use pressure rather than emissivity (where a tracer threshold is applied) for these maps because the discontinuities imposed by the tracer threshold cause problems for the three-dimensional contouring algorithm.

(ii) `yt.OffAxisSlicePlot`: This is used to create two-dimensional (2D) slices through the jet stream and two peaks in pressure within a 50 kiloparsec square. This slice was used to create plots of emissivity, pressure, density, velocity, and divergence.

(iii) `yt.ProjectionPlot`: Three-dimensional line-of-sight projection on to a 2D plane of emissivity either along some arbitrary axis or constrained by the off-axis slices through the pressure maxima.

¹<http://plutocode.ph.unito.it>

²<https://yt-project.org>

Table 1. Table showing the events and representative simulations and timings. The simulation naming convention is precession cone opening angle, injection Mach number, precession period, and resolution.

Event	Simulation	Start frame	End frame
Hotspot splitting	45_100_1_VHR	42	66
Stream splitting	45_100_1_VHR	118	131
Chevron spots	45_100_02_VHR	78	98

2.2 Radio observations

The recent completion of Low-Frequency Array (LOFAR) Two-metre Sky Survey Data Release 2 (LoTSS DR2; Shimwell et al. 2022) generated a catalogue that covered 5700 deg^2 of the Northern

sky and produced 4.4 million extragalactic radio sources. At the time of writing, approximately 85 percent of these sources have been associated with optical IDs through a combination of likelihood-ratio cross-matching and citizen science visual inspection through the Radio Galaxy Zoo (LOFAR) project. We used optically identified, large, bright sources from this catalogue to search for objects that exhibit signs of possibly precession-driven behaviour as discussed in Section 4.

3 RESULTS

In the following subsections, we describe in detail and discuss three of the many multiple hotspot events that are seen in our simulations. For each event, we show three-dimensional contours of the pressure

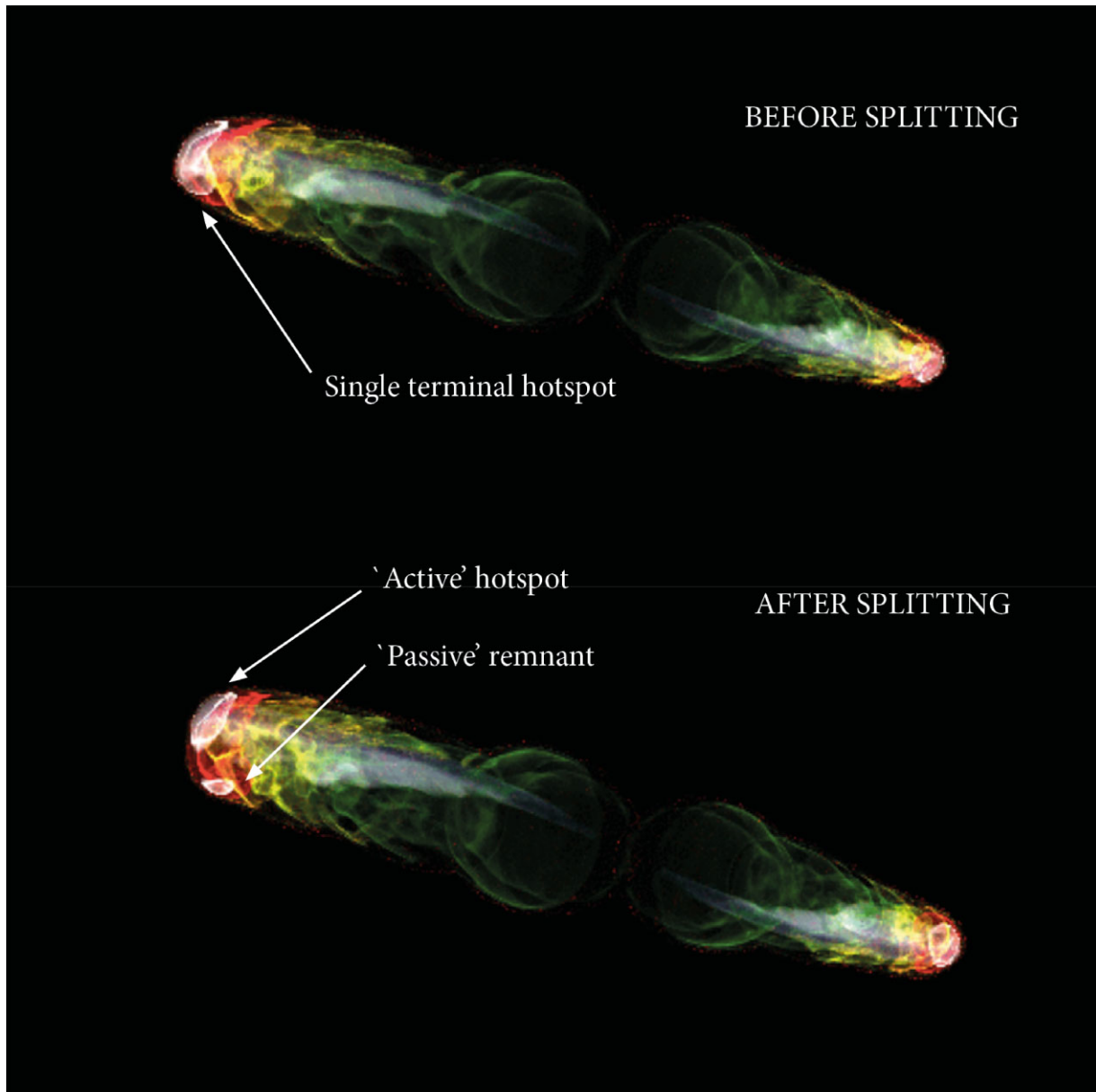


Figure 1. Top panel: A fast jet creates an FRII-style hotspot region where the jet terminates (time-step 44). Bottom panel: As the jet precesses, the hotspot breaks up (time-step 50). The smaller hotspot shrinks and recedes along the contact discontinuity as the lobe expands in the opposite direction. The pale shaded internal region represents the jet as determined from the Mach number. Isobaric surfaces are used to visualize lobes and hotspots. The white contours at the edge of the lobes are the regions of highest pressure and are used to indicate hotspots.

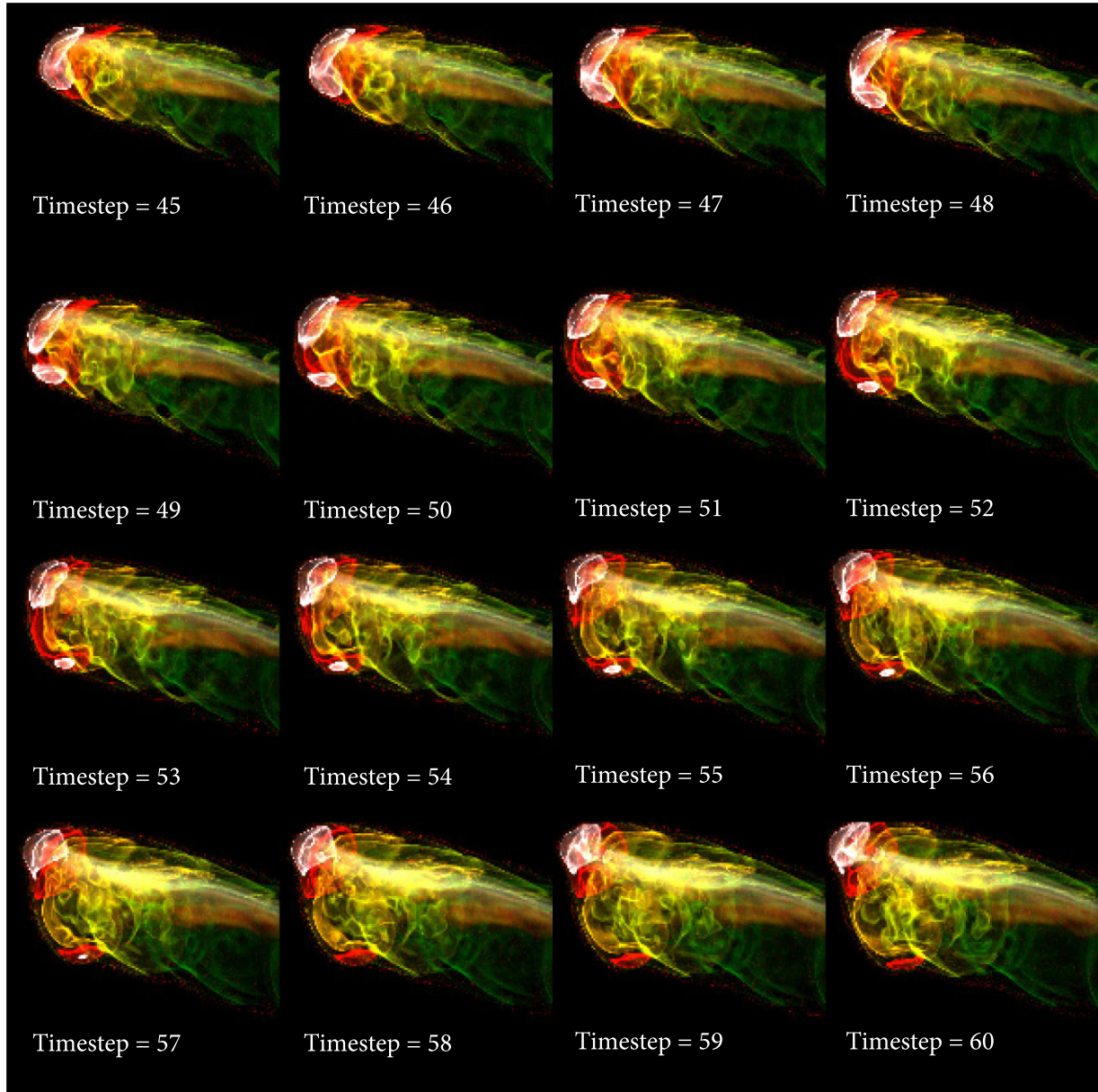


Figure 2. As Fig. 1, showing the evolution of the hotspot splitting event, running from time-steps 45 to 60 representing a duration of 1.8×10^6 yr.

in the simulation as well as projected emissivity (the view seen by an observer from some arbitrary angle) and appropriate slices in physical quantities. The labelling of the simulations follows H20. A given run will be denoted by $\psi_M_pp_res$, where ψ is the precession cone opening angle in degrees, M is the external Mach number, pp is the precession period (1 meaning one complete turn per simulation time), and res denotes the resolution of the simulation where ‘VHR’ stands for ‘very high resolution’. While we ran simulations for a variety of settings (including jets with no precession), the ones presented in this paper are from more ‘extreme’ precession parameters, such as a wide angle for ψ and/or rapid pp , as these show the new mechanisms more distinctly. In what follows, we refer to a given set of simulation outputs (which are saved at regular simulation time intervals) as a ‘time-step’.

3.1 Hotspot splitting

For this event, in simulation 45_100.1_VHR, during the time range specified in Table 1, the simulation initially shows a large terminal hotspot forming as would be expected for an FR II radio jet. As the jet precesses and the lobe expands, this hotspot splits into two components. We name these the ‘active’ and ‘passive’ hotspots, h_A and h_P , and they can be seen in Fig. 1, which shows pressure contours from the beginning and end of the hotspot splitting event. The full evolution of this event can be seen in Fig. 2. Fig. 3 shows a 3×3 grid of the development of the hotspot splitting event from the first time-step where two distinct peaks can be found (top row, time 43), through to a point close to the end where h_P is noticeably diminished but still visible (time 57); here, the first column shows modelled emissivity

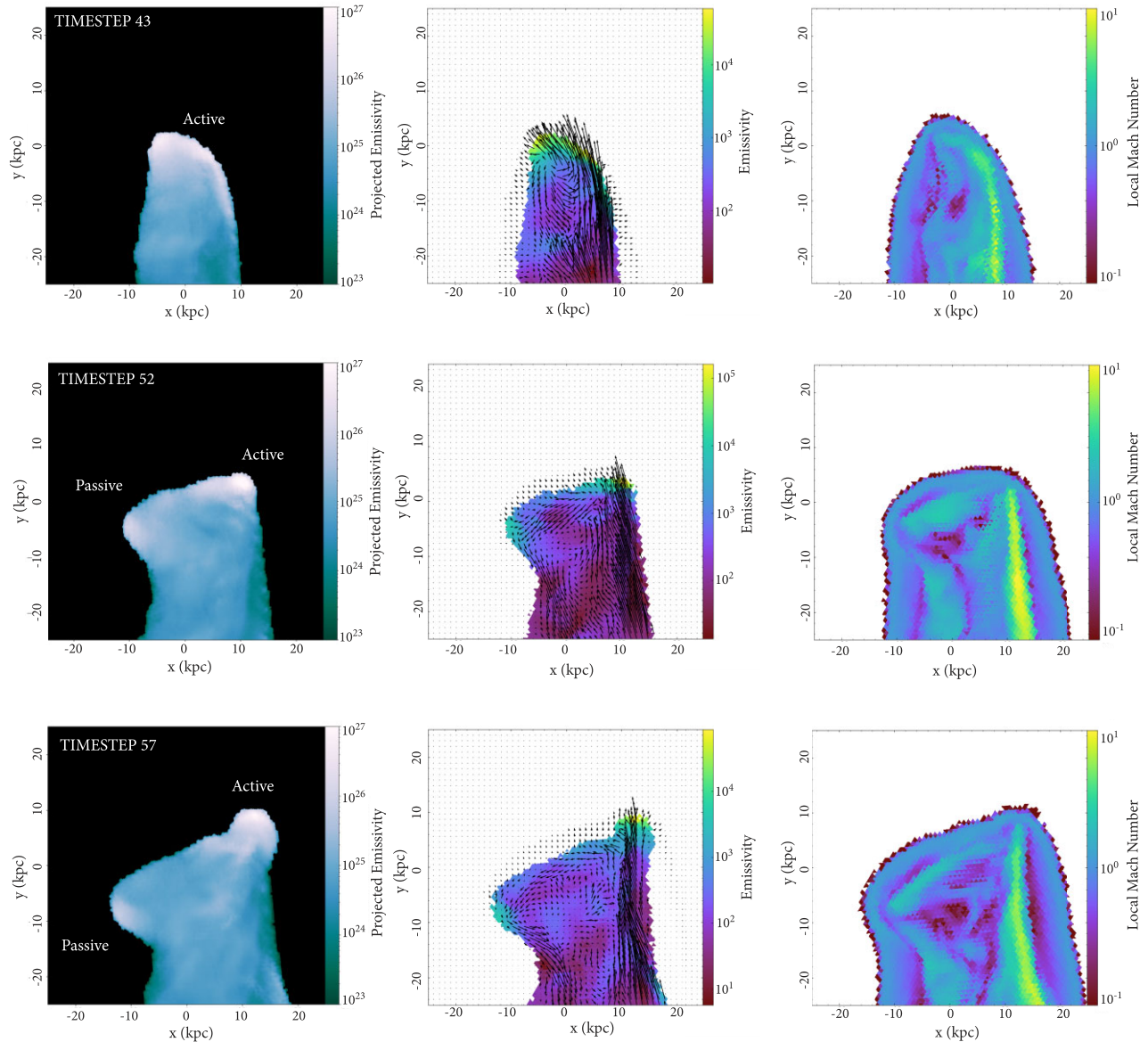


Figure 3. Evolution of hotspot development from beginning of hotspot separation event (top row, simulation time-step 43), middle (middle row, simulation time-step 52) to end (bottom row, time-step 57). First column shows projected emissivity. Second column shows emissivity slices with overlaid velocity vectors. Third column shows the local Mach number. The slices correspond to the lobe to the south lobe seen in the pressure contours of Fig. 1. The contact boundary has been masked out of the emissivity to show only processes internal to the lobe.

of the whole source, the second column shows a slice in emissivity through the two hotspots with overplotted velocity vectors, and the third shows the same slice through the divergence of the velocity field. As can be seen in these images, the ‘active’ hotspot remains at the jet terminus and is the site of the continued jet termination shock. The passive hotspot h_P is not an ongoing shock or significant site of compression (negative divergence) but is simply a remnant of the original large overpressured hotspot. The outflow from h_A pushes h_P along the inside of the contact discontinuity back down towards the core while continuing to confine it. Over time the central compact region of the passive hotspot h_P shrinks, while the rest of it expands and diminishes until h_P is no longer visible.

The evolution of the peak pressure in the two hotspots and their separation is shown in Fig. 4, where we see the pressure in the passive hotspot falling to equal the ambient pressure at the head of the lobe

over the duration of the event. Following Cox et al. (1991), we define the adiabatic expansion time-scale as the sound crossing time for the secondary hotspot, $t = d/v_s$ where v_s is the local sound speed. In physical units as defined in our earlier paper (H20), the hotspot diameter d is around 1.5 kpc and the local sound speed is ~ 30 times the simulation unit of speed, or $1.4 \times 10^4 \text{ km s}^{-1}$. This gives an adiabatic expansion time-scale of $\sim 10^5 \text{ yr}$, which is comparable to a single time-step of the simulation for a hotspot of this size. Clearly as the passive hotspot persists for $\sim 2 \times 10^6 \text{ yr}$, as shown in Fig. 4, it is not freely expanding, consistent with the idea that the outflow from h_A confines h_P without generating an active shock. Contrary to the models discussed in Section 1, we see that the compact hotspot neither signifies the previous location of the jet nor is it formed by a shock in the backflow. This ‘hotspot splitting’ mechanism is related to, but distinct from, to the ‘dentist’s drill’ and ‘splatter-spot’ hotspot

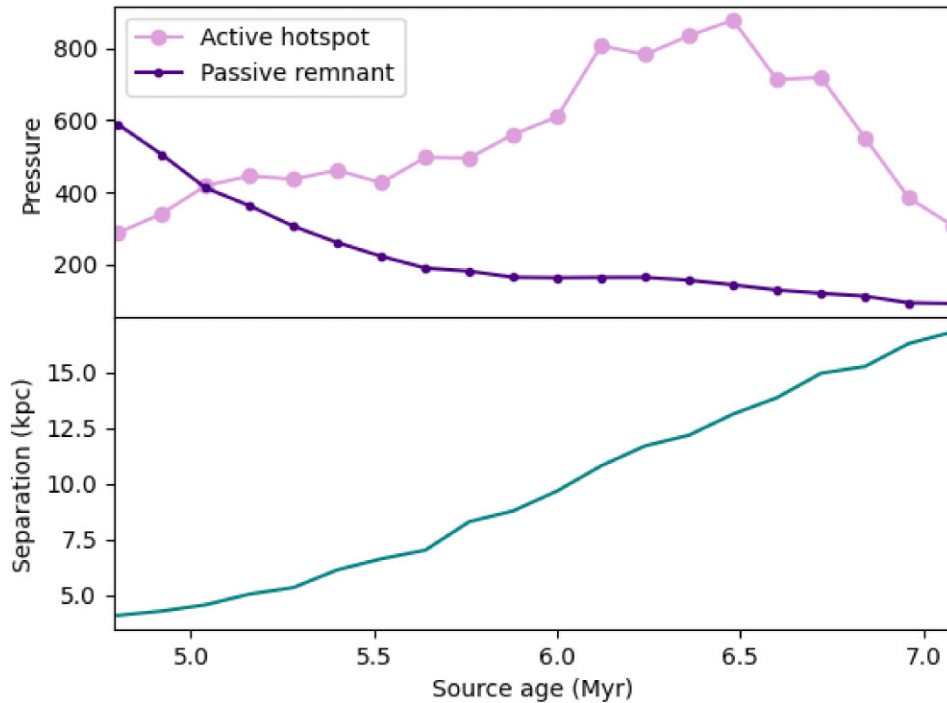


Figure 4. Evolution in active (h_A) and passive (h_P) hotspots before and after hotspot splitting. Top panel shows evolution of pressure in simulation units in the ‘active’ hotspot (pink) and ‘passive’ remnant (purple). Bottom panel shows increasing distance between hotspots as the splitting event continues.

formation models. For example, there is another disconnection event starting at Time-step 59, which could be described in terms of the dentist’s drill model since a new jet termination point is established and the jet no longer reaches the site of the previous hotspot. In this event, the adiabatic expansion results in a fading time of around five time-steps, which is expected given the much larger size of the remnant; this is much shorter than the persistence time of the passive hotspot in the hotspot-splitting scenario.

We note that the hotspot splitting process described here does not have to be driven by jet precession (we have observed it on very short periods during early stages of non-precessing simulations), but it is more noticeable and longer lasting in slowly precessing jets (our ~ 1 simulations), and has a distinct evolution that is absent in non-precessing sources. The wider the precession cone opening angle ψ , the more noticeable the hotspot splitting and the more pronounced the differences in physical properties between h_A and h_P . Therefore, the greater the differences between the two hotspots, the more plausibly they are associated with a strongly precessing source. Many double hotspots seen in well-known radio sources (e.g. 3C 173.1 N, which strikingly resembles the emissivity plots of Fig. 4, or 3C 20 E, Hardcastle et al. 1998) could be explained at least as well by this mechanism as by previously described models such as splatter spot or dentist’s drill.

3.2 Stream splitting and velocity structure

The second event of Table 1 shows one of many regular ‘stream splitting’ events, illustrated in the pressure contours of Fig. 5. During this time period, the jet interacts with the lobe boundary, resulting in the entrainment of dense material which breaks the jet path into two or more component parts which then continue travelling almost in parallel inside the lobe.

Fig. 6 shows the formation of two terminal hotspots from this split stream, with the columns being (left) the projected emissivity of the whole source, and (middle) density and (right) emissivity slices through the double hotspot in the lower half of the image. While one hotspot is slightly larger than the other, as being connected to more of the high-velocity flow, both are still active termination shocks both in emissivity and in the divergence of the velocity field (not shown). The compression remains throughout the event, for as long as the jet remains split. The splitting is caused by an overdense region of the shocked external medium forcing the jet apart (see density plot in Fig. 6), but this structure can be persistent and long-lasting. The hotspots show little morphological evolution throughout the event, which lasted for approximately $\sim 2 \times 10^6$ yr. Additionally, the jet does not have to be split into only two components: during one ‘slowly’ precessing simulation, the jet split into three distinct streams that broke apart and recombined for around one-third of the total simulation time. Although in this particular case the hotspots appear low down in the lobe, this is the result of projection combined with the precessing jet: in this simulation, the jet is now pushing through previously undisturbed material and so the hotspots are effectively at the end of a newly emerging lobe. The interaction with the shocked external medium may be mediated by fluid dynamical instabilities at the end of the jet; our simulations do not allow us to identify the exact mechanisms (e.g. Rayleigh–Taylor or Kelvin–Helmholtz instability at the contact discontinuity) but this issue would merit further study in simulations making use of realistic environments.

In the projected emissivity maps (Fig. 6, col. 1), we see that the two hotspots can be difficult to distinguish from the surrounding jet material; in this case they appear as two bright filaments extending out from the jet. These might be interpreted as hotspots, jet knots, or lobe filaments in a real-world radio map: of course, without modelling particle acceleration it is difficult to tell how these would realistically

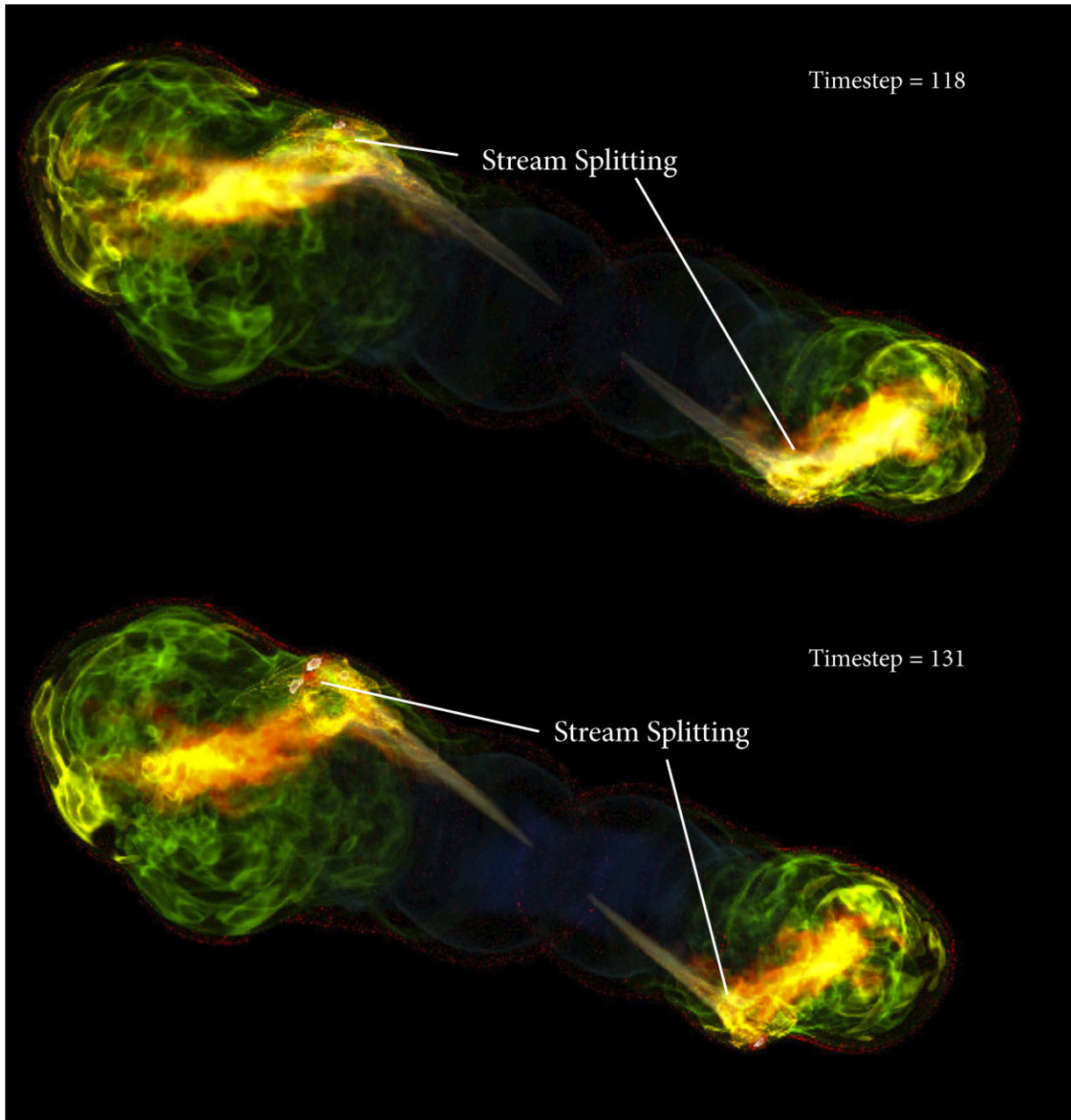


Figure 5. As in Fig. 1 but showing a ‘stream splitting’ event later in the same simulation (time-step 118) Bottom panel: As above, but from time-step 131. Here, the Mach number of the flow is represented by the yellow colours and the regions of highest pressure (hotspots) are represented by the smaller white contours. Some hotspots are hidden by projection and backflow.

appear, but we can see from our plots that they produce a pressure excess and are the sites of active shocks.

As a consequence of the boundary interaction that gives rise to the double hotspots, we also observe complex internal velocity structure. In the later stages of simulations of jets with wide precession cone angles such as this one, we find persistent structures – Mach number ‘clouds’ – where the velocity remains high even long after the jet has precessed away. This is due to the turbulent backflow being deflected by the jet’s initial contact with the lobe boundary right into the centre of the lobe. This is shown by the yellow Mach number structures visible in Fig. 5. These occur whether or not hotspots have formed so long as the flow is fast enough. It is important to note that these flows produce something akin to ‘splatter spots’ as

they result in secondary shocks forming on the opposite side of the lobe. The fact that twin hotspots can create downstream splatter spots highlights that many of these features may be interrelated. The outflow from the twin active hotspots is poorly collimated, resulting in a less distinct, and more diffuse, splatter spot.

The key distinguishing feature of stream splitting would be that particle acceleration would be equally active in two hotspots of similar appearance (unlike the case in hotspot splitting, above, or in dentist’s drill or splatter-spot models) and this could explain the detection of X-ray synchrotron emission, an indicator of ongoing particle acceleration, in several well-studied double hotspots, such as in 3C 227 (Hardcastle et al. 2007). The splitting in the jet itself would only be visible if emissivity and Doppler boosting favoured

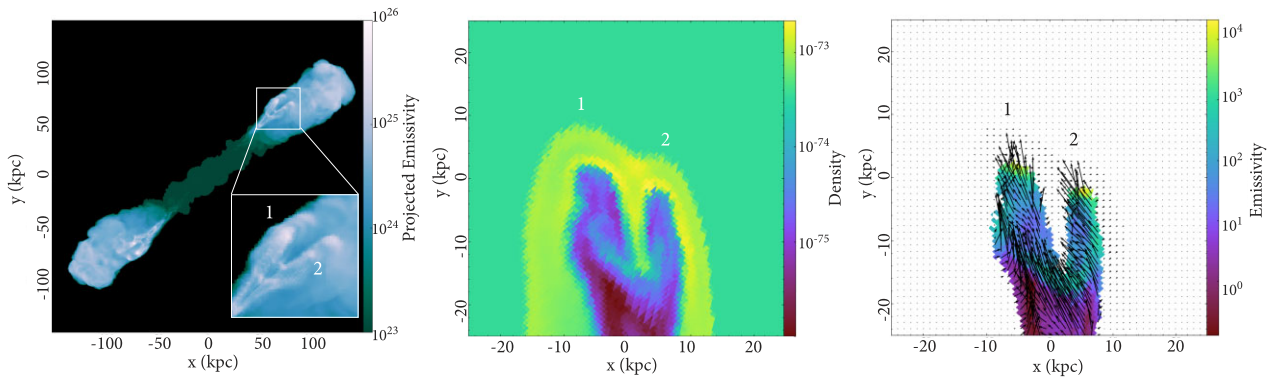


Figure 6. Caption as in Fig. 3, showing the stream splitting event from simulation 45_100.1_VHR at time-step 118. Columns represent projected emissivity (first column) including a cutout of the approximate location of the slices, density slice (middle column), and emissivity slice with velocity vectors (last column). This is one snapshot of an event that corresponds to a duration in physical units of approximately 1×10^7 yr and is just one of many stream-splitting events in this simulation.

it, but there are some objects that could be interpreted in this way, most recently in the images of CGCG 021 – 063 by Fanaroff et al. (2021).

3.3 Chevron spots

In the final example that we select from the simulation 45_100.02_VHR (Table 1), the ‘extreme’ precession of a rapidly precessing jet with a wide precession cone opening angle creates a highly complex and unstable environment. Striking chevron-shaped hotspot regions – which are more akin to dynamic systems or complexes where multiple short-lived hotspots arise from a larger dynamical structure – appear at the base of disrupted jets/plumes, as seen in Fig. 7, which shows the pressure contours for the whole source, and the top panel of Fig. 8, where the projected emissivity is shown. Like the stream splitting events of the previous subsection, the chevrons appear to be created as the precession drives an already-splitting jet into the edge of the lobe. However, these features are distinct because, rather than creating one or more terminal hotspots, the jet transitions to a series of shocks, as can be seen in emissivity, density, and divergence slices through the curved shock regions (Fig. 8, bottom panel). Further into the lobes, the observed structure is unstable and multiple short-lived ‘hotspots’ are visible in emissivity in some time-steps (Fig. 7, bottom panel).

The projected emissivity maps do not consistently preserve the underlying structure that appears in the pressure contours but instead produce highly curved, bright jets that break up often and appear knotty. These often terminate in two distinct hotspot regions. These would be difficult to identify in radio maps resulting in such complex systems going unnoticed. Moreover the curvature of the jet and its brightness are dependent upon the viewing angle of the projected source, rather than any feature of the simulations themselves: the same jet can appear straight from a different angle, and the chevron structures themselves are highly dynamic and unstable. While ‘v-shaped’ or chevron-shaped hotspots are not commonly observed in extragalactic sources, they would only be distinguishable from other structures at high resolution, and there are many objects with bright, curved, and/or discontinuous jets terminating in multiple hotspots. Therefore, it is possible that such features may be overlooked as an indicator of more extreme precession. At low resolution, we might see the chevrons as bright ‘hotspots’ at the base of the lobes combined with complex lobe structure further out, and examples of

this morphology are not uncommon in powerful radio sources, e.g. 3C 215 or 3C 249.1 (Bridle et al. 1994). The large-scale structure of IRAS J1328+2752 (Nandi et al. 2021), a known binary black hole system, is another example of this class.

3.4 Prevalence of different mechanisms

Fig. 9 shows the schematic of five mechanisms for the creation of multiple hotspots: the existing ‘dentist’s drill’ and ‘splatter spots’ plus the three detailed in this paper. It is important to note that these mechanisms are not mutually exclusive. Precessing jet hydrodynamics cause complex internal lobe structures; we observe that more ‘extreme’ simulations (those with shorter *pps* and thus multiple turns throughout the source age) show overlapping events where clusters of multiple hotspots occur in different parts of the lobe from apparently different mechanisms (such as chevron spots leading to splatter spots and so on).

Table 2 shows the prevalence of different formation mechanisms of multiple hotspots in the three different simulations. We have included an ‘unknown’ category where it is difficult to tell where the hotspots are coming from, particularly early in the simulation, or where there is ambiguity in the flow structure. The results of this table appear to show a misleadingly high prevalence of multiple hotspot formation in the non-precessing simulation – however, this occurs very early on in the simulation before the jet becomes stable and produces a single terminal hotspot. The straight jets also expand quickly to run off the grid which means the simulation only runs for half of the length of the other two simulations, so the 32.5 per cent prevalence of multiple hotspots comes from a much shorter simulation and is plausibly an overestimate by a factor ~ 2 . Since the non-precessing jet only shows large, close multiple hotspots early in its lifetime, this is likely caused by interactions with the environment on scales smaller than the jet collimation length-scale, but more simulations are required to confirm this.

The duration and complexity of multiple hotspot generation increases with *pp*. No other parameters are varied. The rapidly precessing (.02) simulations show multiple hotspots for almost 90 per cent of the simulation time, with jets moving from, for example, hotspot splitting to stream splitting as the jet precesses and breaks through the lobe boundary. Rapid precession also brings an increase in unclassifiable events, which are often too small and short lived

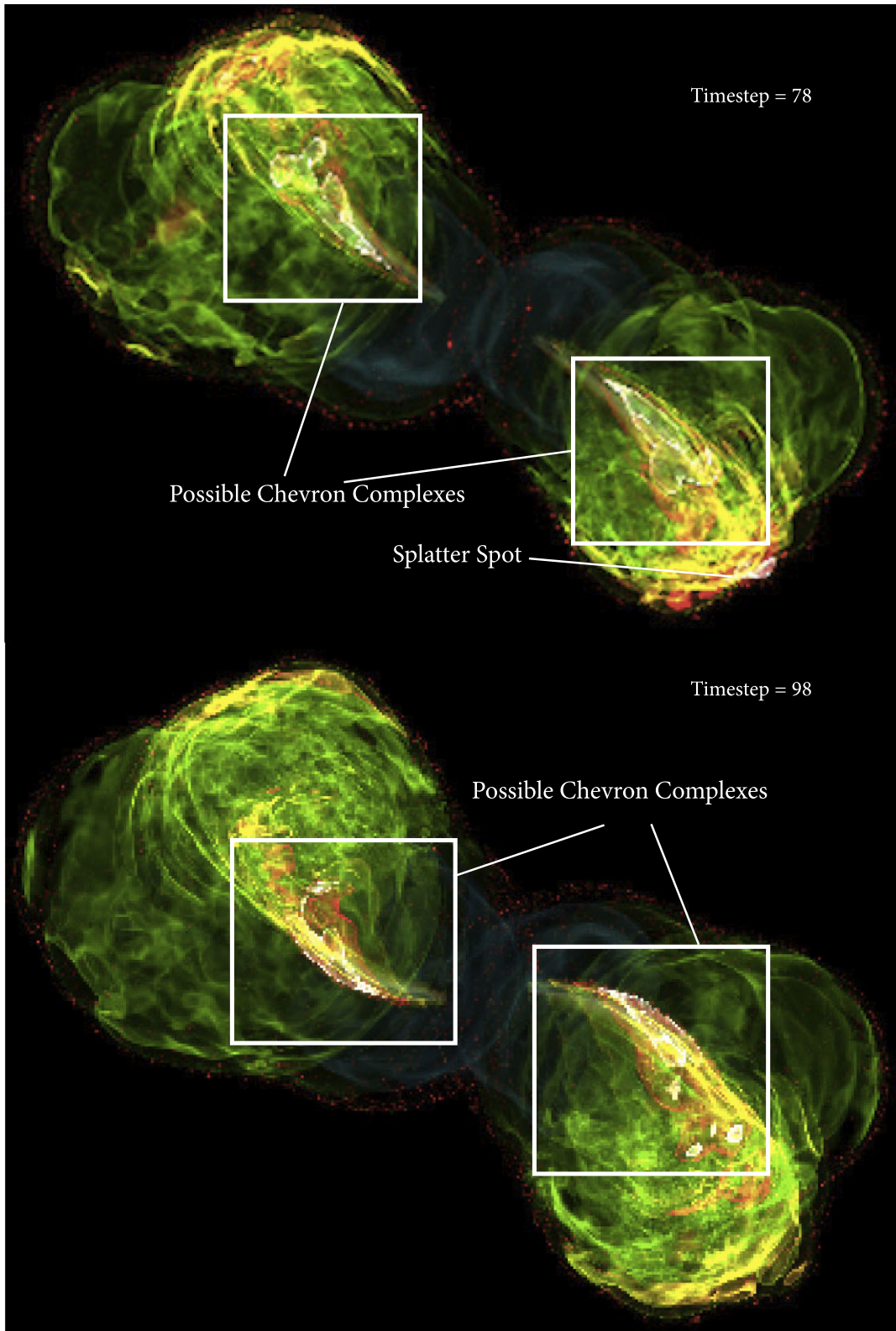


Figure 7. Top panel: White contours show areas of shocks forming chevron-shaped hotspots moving away from the core (simulation 45_100_02_VHR, time-step 78), with possible splatter spot shown at the edge of the lobe. Bottom panel: As above, but the hotspot begins to break up as the precessing jet moves rapidly away from its previous location (time-step 98).

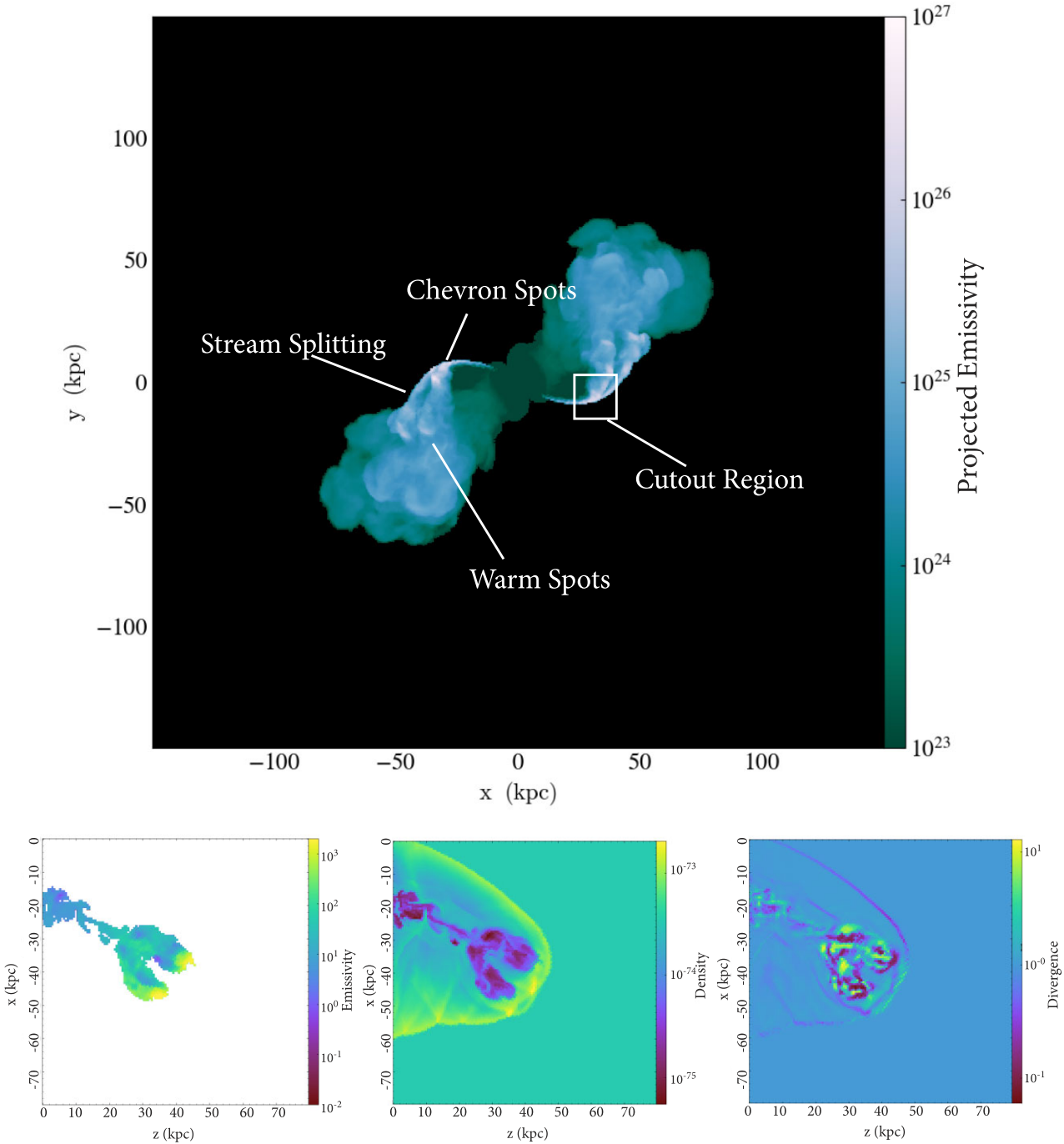


Figure 8. Projected emissivity of chevron structure showing large hotspot complexes in both lobes that would likely be interpreted as bright curved jets. (top panel). Slices through emissivity maximum (bottom left), plus density (bottom middle), and divergence (bottom right) at the same slice position as for the emissivity.

to analyse properly. We observe clusters of hotspot formation in the rapidly precessing clusters that have more than one cause: hotspot complexes close to the jet likely have a different mechanism for their formation than, say, those at the end of the lobe even when occurring in the same frame. We also apparently see a weak evolution of these mechanisms over time, with hotspot splitting generally occurring at earlier times and long periods of stable stream splitting occurring

in the middle of the source lifetime. ‘Chevron’ spots only occur in the rapidly precessing simulation, but can occur at any point in the lifetime of the source.

It is worth mentioning that the mechanisms listed in Table 2 are only recorded if they generate strongly overpressured regions. There are long-lasting events of jet deflection associated with the formation of splatter spots. These do not form ‘hotspot’ structures

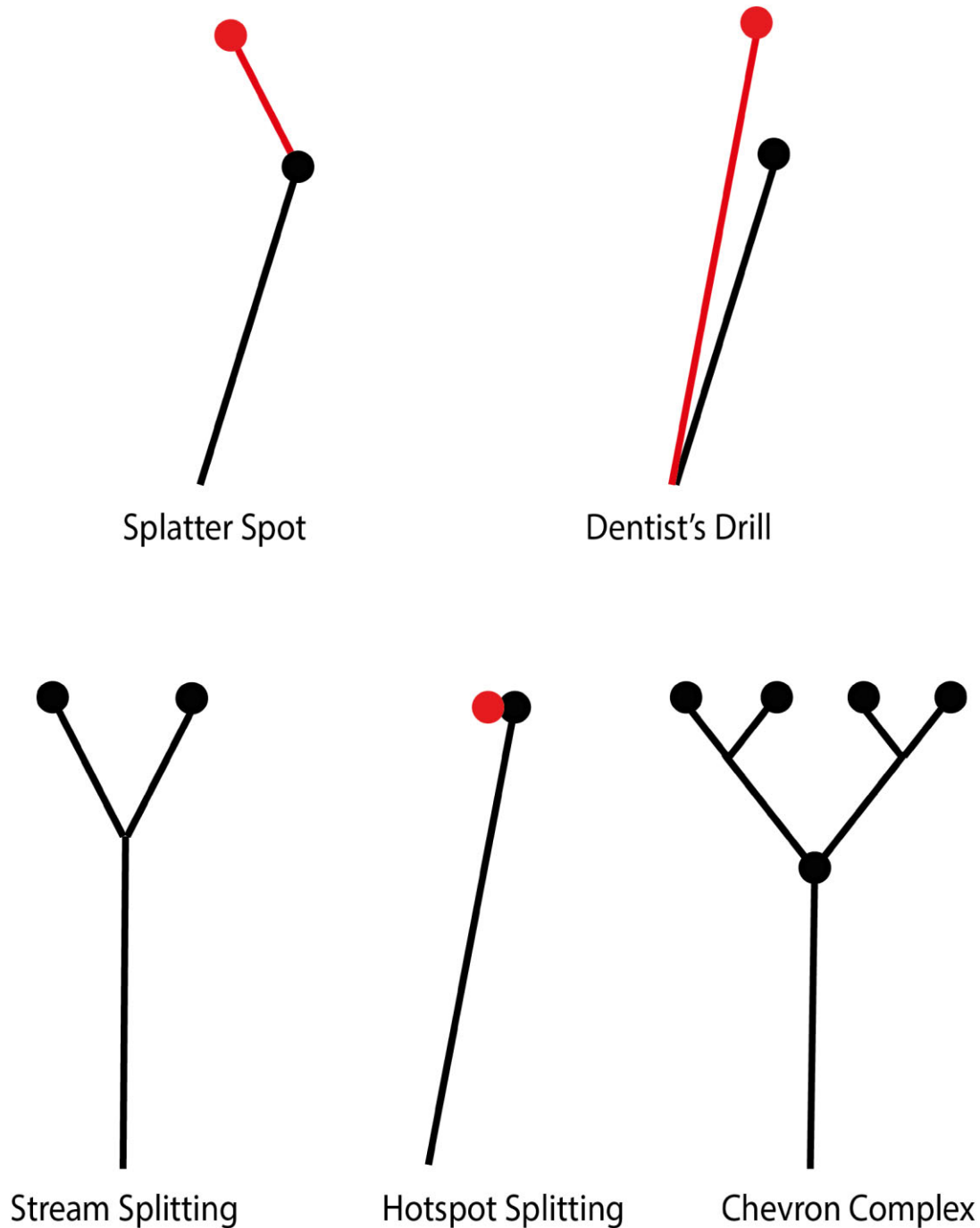


Figure 9. Schematics showing the development of five mechanisms for multiple hotspot generation. Lines indicate the jet and circles indicate the location of terminal hotspots. The lines in black are caused by the current jet flow and red indicates flow and hotspots distinct from the current jet. Top row: Two mechanisms for multiple hotspot formation described in the current literature: splatter spot (left), where a primary flow (black) hits the lobe boundary and deflects into a secondary flow (red) and dentist’s drill (right), where the current flow (black) is distinct from the previous flow (red). Bottom row: The three mechanisms described in this paper: stream splitting (middle) where the jet splits into a stable and long-lasting double flow; hotspot splitting (middle) where a large terminal hotspot breaks into two and the remnant hotspot (red) is slowly forced apart by hydrodynamic forces and chevron complexes (right) where the system generates short-lived, chaotic shocks from an unstable flow structure.

in our simulations but observationally may be visible and associated with ‘warm spots’ (e.g. Leahy et al. 1997).

4 COMPARISON TO OBSERVATIONS

Precessing jets are a useful tool in the hunt for binary supermassive black hole systems and produce predictable morphological changes

to jet paths. In recent years, these have been used to create estimates of the binary separation and gravitational wave strain of certain sources (Krause et al. 2019; Horton et al. 2020a, b). Horton et al. (2020a) in particular highlighted the importance of accurately identifying terminal hotspots in determining a jet path that can be used to constrain binary black hole separation. The mechanisms described earlier were common in our high-resolution

Table 2. Table showing the percentage of time that any of the five stated mechanisms for multiple hotspot formation are visible, plus a category for complex events where it is not possible to identify a formation mechanism. These percentages are taken by visual inspection from a single fixed view and may underrepresent the true time multiple hotspots are present. Superscript *a*: See Section 3.4 for discussion.

Mechanism	._STR	._1	._02
Unknown	3.75 per cent	5.2 per cent	8.8 per cent
Hotspot splitting	5.6 per cent	4.9 per cent	5.10 per cent
Stream splitting	27.5 per cent	34.6 per cent	23.8 per cent
Chevron Spots	0	0	58.1 per cent
Splatter spots	0	0	4.8 per cent
Dentist's drill	0	3.8 per cent	0
Frames with multihotspots	52	138	262
Frames in simulation	160	286	294
Time hotspot visible	32.5 per cent ^a	48.2 per cent	89.1 per cent
Time visible (yr)	6.2×10^6	1.7×10^7	3.1×10^7
Source age (yr)	1.9×10^7	3.4×10^7	3.5×10^7

simulations, suggesting they could be common features of precessing jets.

As a proof of concept, we used the second DR of the LOFAR LoTSS (Shimwell et al. 2022) with preliminary optical identifications to search 10 000 extended sources for a population of large (>2 arcmin), bright (>50 mJy) sources with optical identifications showing precession indicators, namely jet curvature, S-symmetry, jet-lobe misalignment, and multiple hotspots (see H20, for details). Due to resolution issues, we focused on just two of these indicators: curvature and multiple hotspots. After visual inspection of a sample of more than 2000 candidate sources, we selected 112 that showed the above two precession indicators. This population shows a high prevalence of features that can be observed in our simulations.

Fig. 10 shows a selection of 36 radio galaxies taken from the sample of 112 described earlier. Most of these show some suggestion of multiple hotspots or warm spots whether or not they have observable continuous jets. We have not tried to identify the specific mechanisms responsible for multiple hotspot formation, as this would necessarily be subjective and inaccurate. However, some hotspot clusters map more readily on to some of the mechanisms included in the paper; for example, the images shown in (4, 2), (2, 6), and (6, 6) may be indicative of hotspot splitting, and other mechanisms may be present in different images. A detailed exploration of precession characteristics for this population will be covered in a subsequent paper, in which we will make use of higher resolution radio images and the spectra of hotspots in order to suggest formation mechanisms for individual cases.

The availability of the LOFAR data opens up the possibility in future of testing the suggestions of Krause et al. (2019) and Horton et al. (2020a) with a much larger data base. By exploiting the very large data bases of resolved radio sources to be provided by future large-area radio surveys, we may be able to constrain the merger history of supermassive black holes, a key prediction of detailed models of galaxy evolution.

Jet precession may also have an important role to play in the feedback effects of radio active galactic nuclei (AGNs), which are now widely thought to influence the evolution of the galaxy mass function by suppressing cooling in their hot haloes (McNamara & Nulsen 2012). In our simulations, we see that the lobes of precessing jets grow more slowly than non-precessing ones, as jet momentum flux is spread over a larger area (e.g. H20). This means that for a given source age, precessing jets heat material closer to the galactic centre. This may solve a long-standing problem whereby non-precessing jets in simulations tend to spend most of their time heating material with low cooling rates far from the galaxy centre (e.g. Omma & Binney 2004; Hardcastle & Krause 2013). If so, again, it is crucial to identify sources in which precession is taking place using the indicators highlighted in this paper and our previous work.

The processes described in this paper come from simulations designed to mimic plausible *pps* from supermassive black hole binaries. However, there are other ways in which these disturbances can occur on both short and long time-scales. Accretion discs can influence black hole spin direction through the Bardeen–Peterson effect (Lense & Thirring 1918; Bardeen & Petterson 1975), which results in the inner accretion disc aligning with black hole spin axis. Given the chaotic environments at the centres of AGN-producing galaxies, jets can experience perturbations without the presence of a supermassive binary (e.g. Liska et al. 2019). Accretion discs are chaotic environments; whether Bardeen–Peterson precession might dominate earlier in a source lifetime, and thus be more related to features seen in smaller or younger jets, remains unknown.

5 CONCLUSION

Using high-resolution numerical simulations of precessing jets, we have identified three new mechanisms that can produce complex multiple hotspots in powerful radio galaxies. It is important to note that these three mechanisms should be seen as being additional to, rather than replacing, current theories of multiple hotspot formation such as splatter-spots and the dentist's drill model. Both of these prior mechanisms can be seen in our simulations alongside hotspot splitting, stream splitting, and chevron structures. While all three novel mechanisms are linked to precession, particularly in the changes in lobe structure that arise as a consequence, some of these mechanisms – e.g. hotspot splitting – may also occur in non-precessing sources, but to a less extreme degree and for shorter duration. Our work thus supports the argument of Krause et al. (2019) that multiple hotspots in general can be indicators of jet precession, for example, as a result of binary supermassive black hole activity.

This paper focuses on the consequences of ‘extreme’ precession, specifically a 45° precession cone opening angle. However, the listed mechanisms – perhaps with the exception of chevron structures – can also be found in sources with less extreme parameters. In such cases, they may resemble real-world sources (such as Cygnus A, Hercules A, and Hydra A) with multiple hotspots and more typical lobe structure. Given the prevalence of multiple hotspots in real-world sources – as seen by the increase in suitable candidates in LOFAR LoTSS DR2 – more work is necessary to understand which of these possible mechanisms, if any, are at work. A more robust understanding will lead to more realistic constraints (such as binary black hole properties, merger history, and feedback processes) on the nature of the radio-loud AGN population.

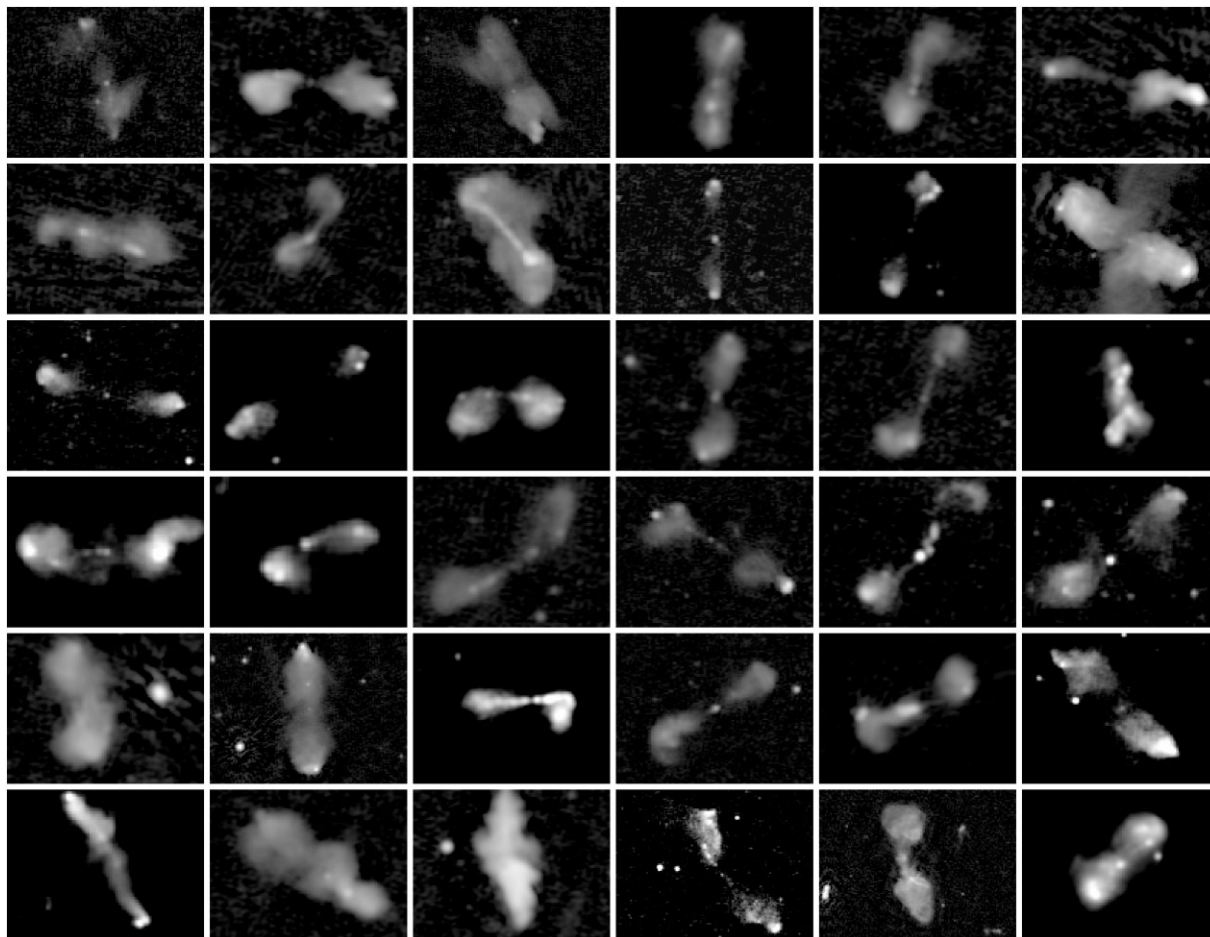


Figure 10. Selection of precessing jet candidate sources in LOFAR LoTSS DR2. Greyscales show total intensity at 144 MHz with a resolution of 6 arcsec. The sources show a selection of precession indicators such as curved jets and multiple hotspots. Numbering used in the text uses rows first followed by columns, with the top row and first column on the left being labelled (1, 1), and the last image in the bottom row being (6, 6).

ACKNOWLEDGEMENTS

MAH acknowledges a studentship from the Science and Technology Facilities Council (STFC) (ST/R504786/1) and support from STFC grants ST/R000905/1 and ST/X002543/1. MJH acknowledges support from STFC grants ST/R000905/1, ST/V000624/1, and ST/X002543/1. Simulations were performed on the University of Hertfordshire High Performance Computing cluster.³ Radio observations were taken from the LOFAR LoTSS DR2. LOFAR was designed and constructed by ASTRON and operated by the ILT foundation under a joint scientific policy. The ILT resources have benefitted from the following recent major funding sources: CNRS-INSU, Observatoire de Paris, and Université d'Orléans, France; BMBF, MIWF-NRW, and MPG, Germany; Science Foundation Ireland (SFI) and Department of Business, Enterprise and Innovation (DBEI), Ireland; NWO, the Netherlands; The Science and Technology Facilities Council, UK; Ministry of Science and Higher Education, Poland; and The Istituto Nazionale di Astrofisica (INAF), Italy. The authors would like to express their sincere gratitude to the anonymous reviewer for their very helpful suggestions for improving this paper.

³<https://uhhpc.herts.ac.uk/>

DATA AVAILABILITY

No new observational data were generated or analysed in support of this research. Simulation source files are available on request. LoTSS DR2 images can be downloaded from <https://lofar-surveys.org/>.

REFERENCES

- Bardeen J. M., Petterson J. A., 1975, *ApJ*, 195, L65
 Begelman M. C., Blandford R. D., Rees M. J., 1980, *Nature*, 287, 307
 Bridle A. H., Hough D. H., Lonsdale C. J., Burns J. O., Laing R. A., 1994, *AJ*, 108, 766
 Carilli C. L., Bartel N., Linfield R. P., 1995, Astronomy Data Image Library, VLBI Observations of the Nuclear Jet in Cygnus A, Astronomy Data Image Library, October 1995
 Cox C. I., Gull S. F., Scheuer P. A. G., 1991, *MNRAS*, 252, 558
 Ekers R. D., Fanti R., Lari C., Parma P., 1978, *Nature*, 276, 588
 Fanaroff B. L., Riley J. M., 1974, *MNRAS*, 167, 31P
 Fanaroff B. et al., 2021, *MNRAS*, 505, 6003
 Gower A. C., Gregory P. C., Unruh W. G., Hutchings J. B., 1982, *ApJ*, 262, 478
 Hardcastle M. J., Krause M. G. H., 2013, *MNRAS*, 430, 174
 Hardcastle M. J., Krause M. G. H., 2014, *MNRAS*, 443, 1482
 Hardcastle M. J., Looney L. W., 2001, *MNRAS*, 320, 355
 Hardcastle M. J., Alexander P., Pooley G. G., Riley J. M., 1998, *MNRAS*, 296, 445

- Hardcastle M. J., Croston J. H., Kraft R. P., 2007, *ApJ*, 669, 893
- Hardee P. E., Norman M. L., 1990, *ApJ*, 365, 134
- Horton M. A., Hardcastle M. J., Read S. C., Krause M. G. H., 2020a, *MNRAS*, 493, 3911
- Horton M. A., Krause M. G. H., Hardcastle M. J., 2020b, *MNRAS*, 499, 5765 (H20)
- Kaiser C. R., Alexander P., 1997, *MNRAS*, 286, 215
- Krause M. G. H. et al., 2019, *MNRAS*, 482, 240
- Laing R., 1982, in Heeschen D. S., Wade C. M., eds, Proc. IAU Symp. Vol. 97, Extragalactic Radio Sources. Kluwer, Dordrecht, p. 161
- Laing R., 1989, in Meisenheimer K., Roeser H.-J., eds, Hot Spots in Extragalactic Radio Sources, Vol. 327. European Southern Observatory, Garching, p. 27
- Leahy J. P., Black A. R. S., Dennett-Thorpe J., Hardcastle M. J., Komissarov S., Perley R. A., Riley J. M., Scheuer P. A. G., 1997, *MNRAS*, 291, 20
- Lense J., Thirring H., 1918, *Phys. Z.*, 19, 156
- Liska M., Tchekhovskoy A., Ingram A., van der Klis M., 2019, *MNRAS*, 487, 550
- Lonsdale C. J., Barthel P. D., 1986, *AJ*, 92, 12
- McNamara B. R., Nulsen P. E. J., 2012, *New J. Phys.*, 14, 055023
- Mignone A., Bodo G., Massaglia S., Matsakos T., Tesileanu O., Zanni C., Ferrari A., 2007, *ApJS*, 170, 228
- Nandi S., Caproni A., Kharb P., Sebastian B., Roy R., 2021, *ApJ*, 908, 178
- Omma H., Binney J., 2004, *MNRAS*, 350, L13
- Scheuer P. A. G., 1982, in Heeschen D. S., Wade C. M., eds, Proc. IAU Symp. Vol. 97, Extragalactic Radio Sources. Kluwer, Dordrecht, p. 163
- Shimwell T. W. et al., 2022, *A&A*, 659, A1
- Smith M. D., 1984, *MNRAS*, 211, 767
- Valtaoja E., 1984, *A&A*, 140, 148
- Williams A. G., 1985, *Observatory*, 105, 224

This paper has been typeset from a $\text{\TeX}/\text{\LaTeX}$ file prepared by the author.